Molecular Dynamics of a Laser-Annealing Experiment

Charles L. Cleveland, Uzi Landman, and R. N. Barnett
School of Physics, Georgia Institute of Technology, Atlanta, Georgia 30345

(Received 12 July 1982)

A study of a laser-annealing system using a new molecular dynamics method modified to faithfully simulate typical experimental conditions is presented. Following melting, the recrystallization interface is layer structured in the melt. Rapid recrystallization, impurity segregation and constitutional undercooling, and the dynamics of the processes are demonstrated.

PACS numbers: 61.50.Cj, 64.75.+g, 66.70.+f, 68.45.-v

The processing of materials (semiconductors or metals) by using laser or electron beams, generically called "laser annealing,"[1,2] provides novel techniques of crystal growth, damage recovery, and preparation of alloys of nonthermodynamic compositions. Aside from the varied important potential technological applications, the physical processes occurring in materials subject to intense radiation and the underlying mechanisms of ultrahigh-speed crystallization under conditions which could be far from equilibrium present an enormous theoretical challenge. The theoretical issues involve[3] (a) the nature of the coupling of radiation (photons, particles) to solids, (b) thermodynamics, in particular nonequilibrium and stability analysis (metastability, morphological stability[4]), (c) rapid solidification kinetics, and (d) dynamics. All theoretical efforts to date are based[3] on continuum phenomenological treatments of particle diffusion and heat flow (moving boundary problem), which while providing useful insight do not allow understanding of the dynamics and the atomic-scale processes which govern the kinetics. In this note we present the first theoretical investigation which addresses, and reveals, certain of the atomistic processes which underlie fast solidification phenomena under "laser-annealing" conditions. Additionally, we demonstrate the unique value of molecular dynamics (MD) simulation analysis in studies of material processes of unusual nature.

Prior to the presentation of results we outline certain of the pertinent features of the simulation. (i) The simulated system consists of a slab with thirty atomic planes (fifty atoms per plane, initial average layer spacing ~2.7 Å) forming an fcc crystal with the (100) face exposed. One side of the slab (starting at $z=0$) interacts with a static extension of the crystal and the other side is free in the z direction. Two-dimensional periodic boundary conditions are imposed on the planes with the $\vec{a}$ and $\vec{b}$ vectors defining the basis of the MD cell treated as dynamical variables,[5] thus allowing variations in both areal density and thickness. (ii) The incident beam, on the free side of the system, has a triangular intensity-versus-time profile, 1.6 psec in duration and carrying a total energy of 6.3×10^{-5} J/cm^2. The coupling of the beam energy to the lattice modes is simulated via a time-stepwise scaling of particle velocities for the duration of the pulse using an absorption profile given by $\exp[0.02z/(1\ \text{Å})]$, where z in angstroms increases going out of the solid. (iii) The initial system consists of two species, 90 at.% of species α with species β substituted randomly, interacting via 6-12 Lennard-Jones potentials

$$V_{\alpha\beta}(r)=4\epsilon_{\alpha\beta}\left[\left(\frac{\sigma_{\alpha\beta}}{r}\right)^{12}-\left(\frac{\sigma_{\alpha\beta}}{r}\right)^{6}\right],$$

with $\sigma_{\alpha\beta}=(\sigma_{\alpha\alpha}+\sigma_{\beta\beta})/2$ and $\epsilon_{\alpha\beta}=(\epsilon_{\alpha\alpha}\epsilon_{\beta\beta})^{1/2}$. We choose $\sigma_{\beta\beta}/\sigma_{\alpha\alpha}=1.07$, $\epsilon_{\beta\beta}/\epsilon_{\alpha\alpha}=1.387$, and mass ratio $m_\beta/m_\alpha=2.098$ [corresponding to argon (α) and krypton (β) parameters; $\sigma_{\mathrm{Ar}}=3.4$ Å]. Reduced units are used: temperature $T^*=k_BT/\epsilon_{\alpha\alpha}$ and reduced length $=L/\sigma_{\alpha\alpha}$. The system is initially equilibrated at $T^*=0.4$ (the melting temperature of pure bulk α is $T_{m,\alpha}{}^*=0.7$). The integration time step is $\Delta t=0.0075t_\alpha$, where $t_\alpha=2.16$ psec for Ar. (iv) Heat conduction to the underlying substrate reservoir is simulated by scaling velocities in the bottom two layers according to $\dot{Q}(t)=A\kappa(T(t))\,dT(t)/dz$, where A is the planar area and $\kappa(T(t))$ is a temperature-dependent heat conductivity taken from solid-Ar experimental data.[6] The gradient $dT(t)/dz$ is temporally determined by a linear extrapolation of the system temperature profile to a point in the substrate, distant from the bottom of the slab by $31.56\sigma_{\alpha\alpha}=107.5$ Å (different substrate material or temperature will yield different gradients).

To facilitate the presentation of results we define for any property g_i which depends on the phase-space point $(\vec{r}_i,\vec{v}_i)$ of atom i located at z_i,

a local density (per unit length) of that property at z by

$$\hat{\rho}_g(z) = (2\pi)^{-1/2}\sigma^{-1}\sum_i g_i \exp[-(z - z_i)^2/2\sigma^2],$$

with $\sigma = 0.126$ of the average layer spacing. For particle number density (per length) profile ($g_i = 1$), $\hat{\rho}_n(z) \equiv \rho(z)$. In the following we present the per-particle property local densities $\rho_g(z) \equiv \hat{\rho}_g(z)/\rho(z)$. For the kinetic energy, KE, and potential energy, PE, $g_i = \frac{1}{2}m_i v_i^2$ and $\frac{1}{2}\sum_j V(|\vec{r}_i - \vec{r}|)$, respectively. The kinetic temperature is given by two-thirds of the KE. An additional quantity of interest is the planar orientational order parameter[7] O_4 for which

$$g_i = W_i^{-1} \sum_{j \in \mathrm{nn}(i)} W_{ij} \exp(i4\theta_{ij}),$$

where $W_i = \sum_{j \in \mathrm{nn}(i)} W_{ij}$, $W_{ij} = \exp(z_j - z_i)^2/2\sigma_0^2$, $\sigma_0 \simeq 0.5$ layer spacing, and nn(i) denotes nearest neighbors to atom i. θ_{ij} is the angle that the "bond" between atoms i and j makes with the x axis. The absolute value of O_4 attains a value close to unity on a (100) face of an fcc layer, and is close to zero for a liquid.

In Figs. 1(a) and 1(b) the particle density, KE, PE, and $|O_4|$ vs z are shown for the initial system and immediately at the end of the 1.6-psec heat pulse. The minima in the PE profile occur at the location of atomic planes. It is seen [Fig. 1(b)] that while the kinetic energy is increased because of the pulse, disordering has just started to occur since not enough time has elapsed yet for thermal energy to be converted to potential energy. The initial random impurity distribution is shown in Fig. 1(d)(i). In Fig. 1(c) time-aver-

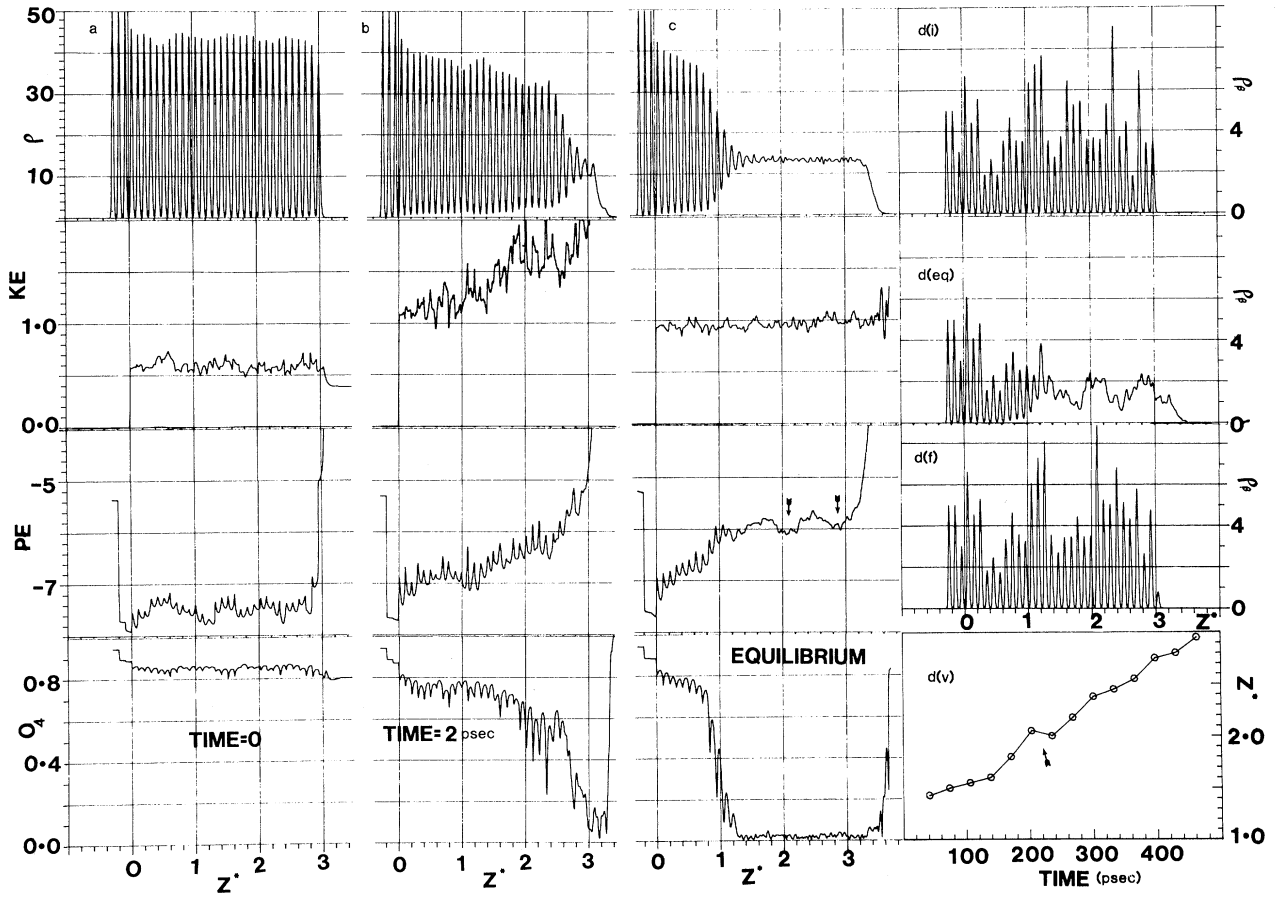

FIG. 1. (a)–(c): Profiles of number density (ρ), KE, PE, and $|O_4|$ vs $z^* = z/7.89\sigma_{\alpha\alpha}$ for the initial system, at the termination of the pulse, and for an isolated equilibrium system, respectively. (d)(i), (d)(f), and (d)(eq): Impurity density profiles for the initial, final, and equilibrated systems, respectively. (d)(v): Position, z^*, of the recrystalization interface vs time (in picoseconds). A straight-line fit yields a solidification velocity of 11 m/sec. Detailed analysis indicated that a region characterized by $|O_4| < 0.4$ lacks planar long- and short-range order. This criterion was adopted in the construction of Fig. (d)(v).

aged results are shown for a thermally isolated system ($\kappa = 0$), which has been subjected to an identical heat pulse and let develop for a very long time. In this case, an equilibrated system with solid-liquid coexistence has been produced (equilibrium temperature corresponds to KE of 0.96). Note the sharp drop in O_4 at about $z^* = 1$ indicating loss of *intralayer order* while *permanent layering* in the particle density profile is evident beyond that point into the liquid. The time-averaged impurity distribution in the equilibrated system [Fig. 1(c)] shown in Fig. 1(d)(eq) reveals a feature which indicates a tendency of the impurity to avoid the interface. (This region is characterized by transport coefficients of a liquid.) The corresponding stabilization in these regions is indicated in the PE profile [Fig. 1(c)] by arrows.

Next we turn in Fig. 2 to a sequence of profiles for a heat-conducting system taken at selected time steps during the evolution of the system after the termination of the pulse. Figure 2(a) describes the system at the final stages of melting. As seen in Fig. 2(b) recrystallization started while the kinetic temperature of the melt, T_{liquid}, was still above the solid-liquid coexistence temperature, T_m; see Fig. 1(c). The ρ and $|O_4|$ profiles at 73 psec show clear evidence of a layered melted region, also seen in the PE profile. The moving recrystallization front is characterized by a structured three-dimensional interface, anisotropic in density and properties. The anisotropic structured nature of the interface may play an important role in the recrystallization kinetics and in phenomena such as solute trapping. Once T_{liquid} has dropped to T_m, the velocity of crystallization accelerates. Later, however, at 203 psec [Fig. 2(c)] the velocity of crystallization decreases sharply [Fig. 1(d)(v)] and interface layering temporarily becomes less evident. These changes are associated with an increase in impurity concentration at the interface resulting from the previous expulsion of the impurity into the liquid (and perhaps a tendency for cellular ordering). T_{liquid} subsequently falls below T_m (a manifestation of constitutional supercooling),

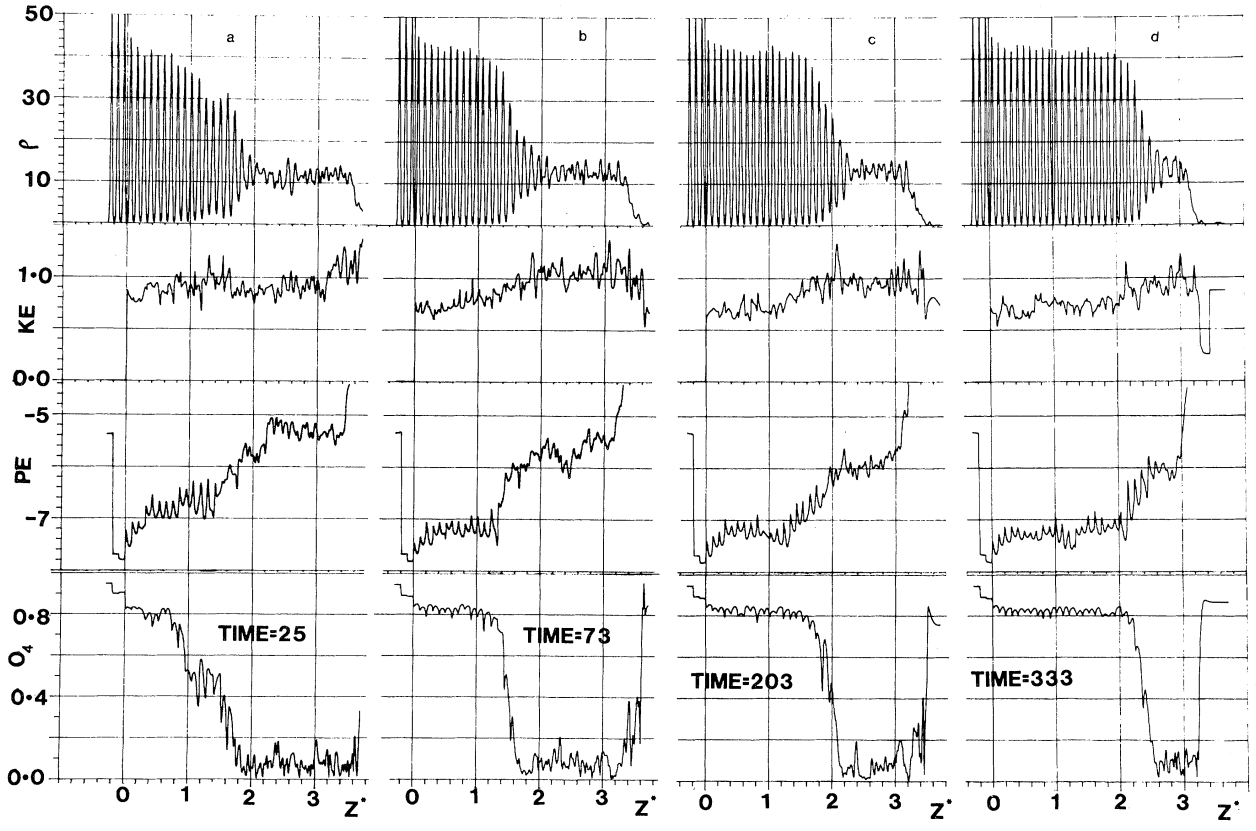

FIG. 2. (a)–(d): Profiles of number density (ρ), KE, PE, and $|O_4|$ vs z^* at time steps 25 (end of melting), 73, 203, and 333 psec, respectively.

the velocity of crystallization recovers, and layering is reestablished [see Fig. 2(d) at 333 psec]. At the end of the process (~500 psec) the total number density profile is identical to that in Fig. 1(a), and the impurity profile is shown in Fig. 1(d)(f). A certain amount of impurity segregation to the free surface is evident.

In this study we demonstrated the use of MD in an investigation of a complex nonequilibrium material process. Of interest is the "liquid layering" which, as we observed, precedes the solidification front, preparing the liquid for formation of perfect crystalline planes, and significantly affects impurity segregation and transport (see also Wood, Ref. 3), while in turn being affected by interfacial conditions that it, in part, brings about. MD studies can be instrumental in analyzing the dynamic interrelationship between the structure and properties of the interface and the solidification process. Investigations continue in our laboratory on the relationship between the time scale of interface processes (such as layering) and the nature of the resulting solid (crystalline versus amorphous) under various solidification rates, the effect of crystal face, crystallization on amorphous substrates, the role of "liquid layering" in solute trapping or expulsion, and the dependence on host and impurity interaction potentials and mass ratios.

This work was supported by U. S. Department of Energy Contract No. EG-S-05-5489.

[1]*Laser and Electron Beam Processing of Materials*, edited by C. W. White and P. S. Peerey (Academic, New York, 1980).

[2]*Laser-Solid Interactions and Laser Processing —1978*, edited by S. D. Ferris, H. J. Leamy, and J. M. Poate, AIP Conference Proceedings No. 50 (American Institute of Physics, New York, 1979).

[3]See Ref. 1, Part I; Ref. 2. For details, see R. F. Wood and G. E. Giles, Phys. Rev. B 23, 2923 (1981); R. F. Wood, J. R. Kirkpatrick, and G. E. Giles, Phys. Rev. B 23, 5555 (1981); R. F. Wood, Phys. Rev. B 25, 2786 (1982).

[4]J. Narayan, in *Microscopy of Semiconducting Materials —1981*, edited by A. G. Cullis and D. C. Joy, IOP Conference Series No. 60 (Institute of Physics, London, 1981), p. 101; A. G. Cullis, D. T. Hurle, H. C. Webber, N. G. Chew, J. M. Poate, P. Baeri, and G. Forti, Appl. Phys. Lett. 38, 642 (1981).

[5]M. Parrinello and A. Rahman, Phys. Rev. Lett. 45, 1196 (1980).

[6]I. N. Krupskii and V. G. Manzhelii, Zh. Eksp. Teor. Fiz. 55, 2075 (1968) [Sov. Phys. JETP 28, 1097 (1969)].

[7]U. Landman, C. L. Cleveland, and C. S. Brown, Phys. Rev. Lett. 45, 2032 (1980).

Domain Walls and the Melting of Commensurate Surface Phases

David A. Huse and Michael E. Fisher

Baker Laboratory, Cornell University, Ithaca, New York 14853

(Received 22 July 1982)

Commensurate adsorbed surface phases, particularly $p \times 1$ rectangular and $\sqrt{3} \times \sqrt{3}$ hexagonal phases, exhibit two (or more) classes of domain wall, reflecting a lower than ideal symmetry; these compete statistically and undergo wetting transitions. Scaling arguments and model calculations indicate that new types of continuous melting transitions, possibly already seen in Kr on graphite, can thereby arise.

PACS numbers: 68.40.+e, 05.70.Fh, 64.70.Dv, 75.10.Hk

Many ($d=2$)-dimensional systems are now known in which an adsorbed, commensurate surface phase, with the adsorbate atoms or molecules in ordered registry with the substrate solid, *melts* under variation of the temperature, T, or chemical potential, ζ (controlled by the vapor pressure). Such melting may be discontinuous (i.e., first order) in nature but theory suggests,[1] and experiments confirm,[2,3] that *continuous transitions* may also occur. We focus here on such continuous $d=2$ commensurate melting and ask "What types of transition may occur?" We argue that a class of asymmetric or chiral transitions —distinct from the previously identified symmetric Ising, Potts, and p-state clock universality classes—should arise in real systems and may already have been seen in studies of krypton on graphite.[3] The existence of *different types of domain walls* plays a significant role in the phenomena.

